Supplementary Information (SI) for Journal of Materials Chemistry A.

Ultra-Wide Temperature Cycle Control Based on Photo-responsive Phase-Change

Jing Ge, [a] Xiaoyu Yang, [a] Zedong Wang, [a] Yiyu Feng, *[a] Wei Feng *[a]

[a]School of Materials Science and Engineering and Tianjin Key Laboratory of Composite and Functional Materials, Tianjin University, Tianjin 300350, P. R. China.

*Corresponding author E-mail:

fengyiyu@tju.edu.cn (Y. Feng)

weifeng@tju.edu.cn (W. Feng)

Supplementary Figures and Results

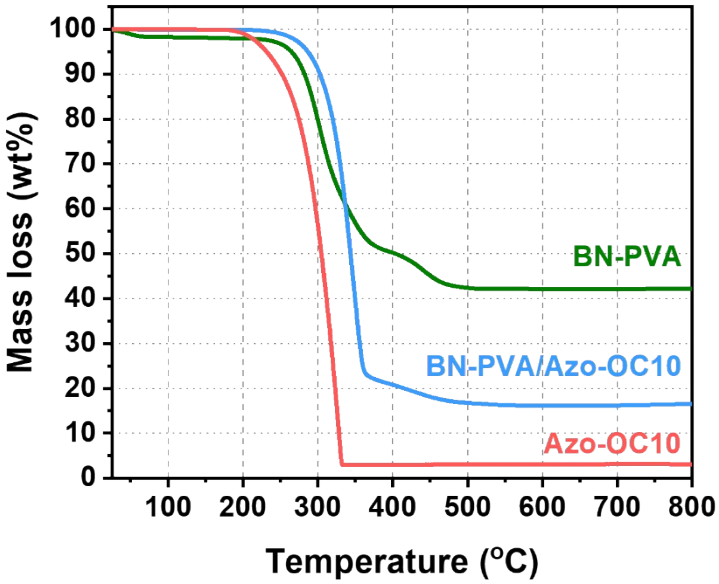

Fig. S1 TGA curves of BN-PVA, BN-PVA/Azo-OC10, and Azo-OC10 (10 °C/min, N_2 atmosphere).

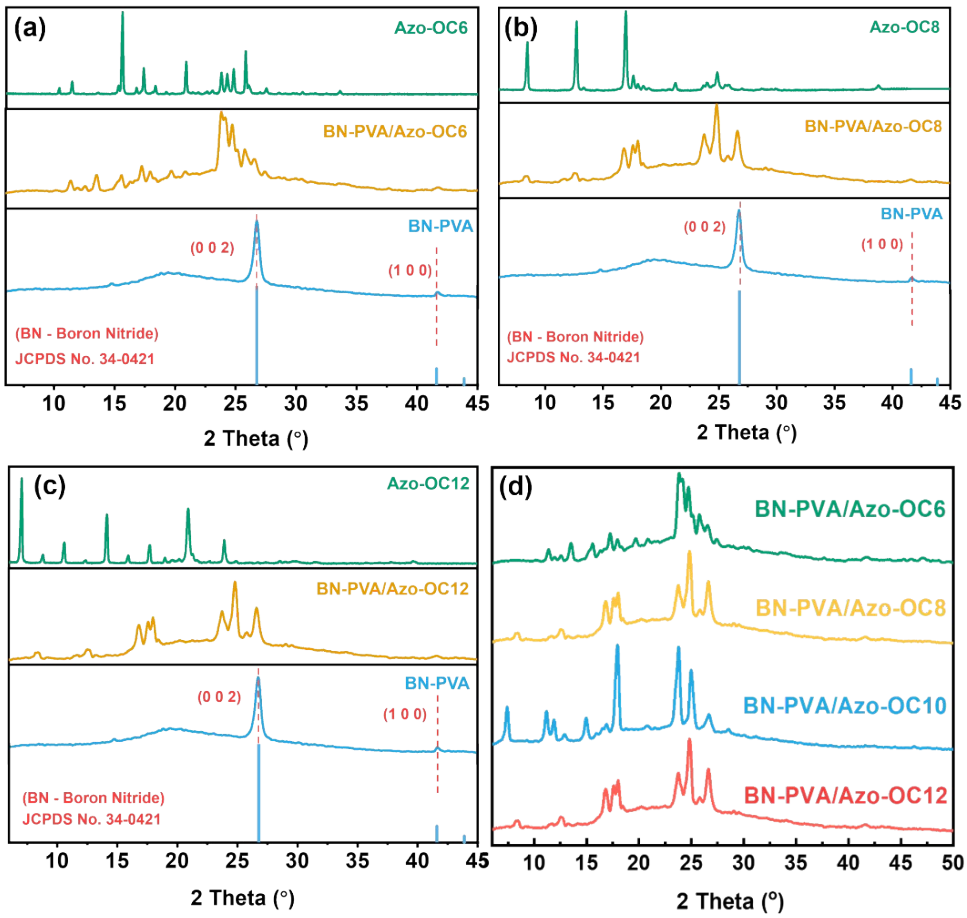

Fig. S2 XRD comparison of (a) Azo-OC6, BN-PVA aerogel, and BN-PVA/Azo-OC6 composite aerogel; (b) Azo-OC8, BN-PVA aerogel, and BN-PVA/Azo-OC8 composite aerogel; and (c) Azo-OC12, BN-PVA aerogel, and BN-PVA/Azo-OC12 composite aerogel at 2θ ranging from 5° to 45°. (d) XRD curves of BN-PVA/Azo-OCn composite aerogels filled with Azo-OCn molecules of different chain lengths (n=6, 8, 10, 12).

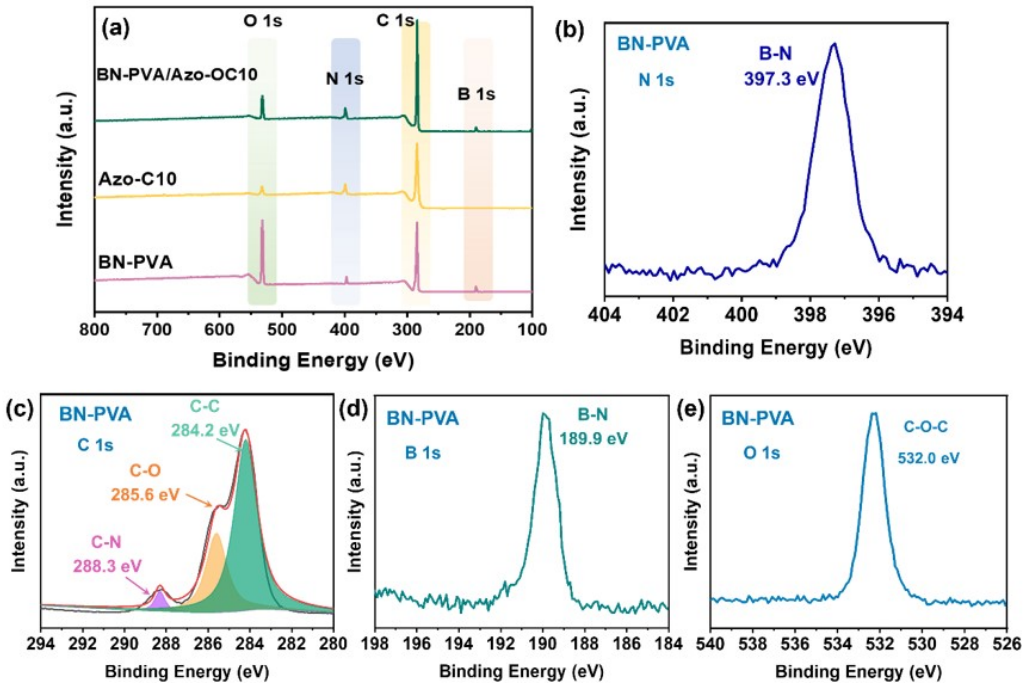

Fig. S3 (a) The wide-scan, N1s, O 1s, B 1s, and C1s core-level XPS spectra of BN-PVA, Azo-OC10, and BN-PVA/Azo-OC10 aerogel samples. (b) N 1s, (c) C 1s, (d) B 1s, and (e) O 1s region spectra of the BN-PVA aerogel.

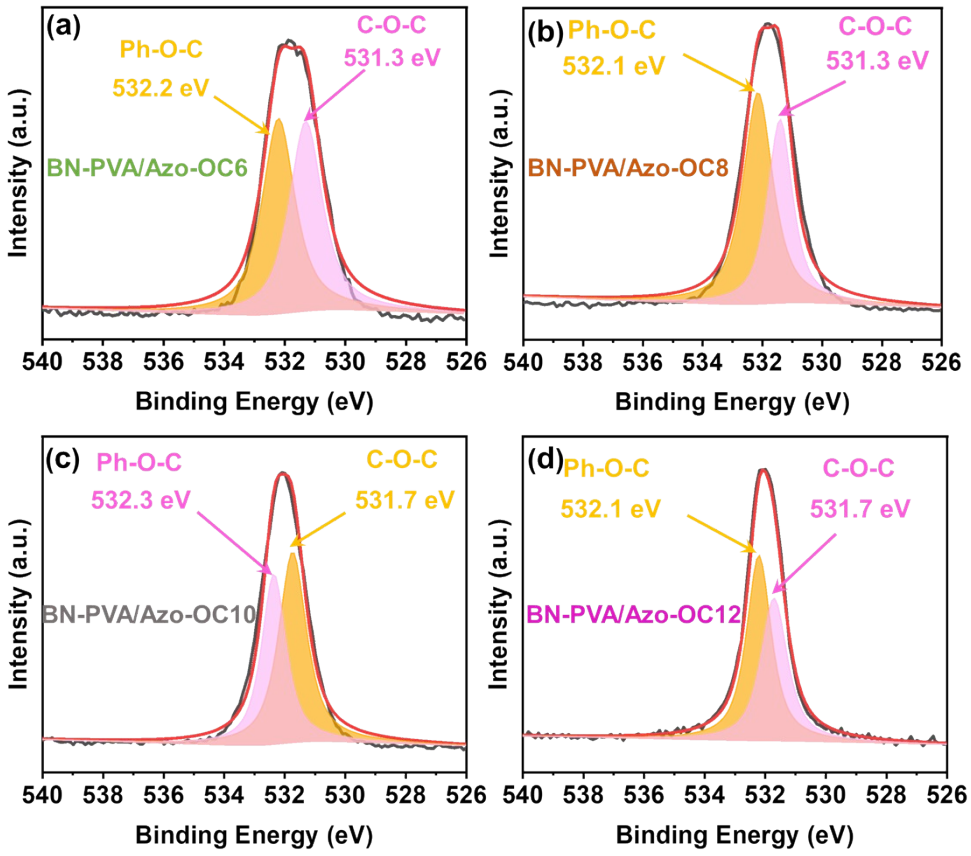

Fig. S4 O 1s XPS spectra of (a) BN-PVA/Azo-OC6, (b) BN-PVA/Azo-OC8, (c) BN-PVA/Azo-OC10, and (d) BN-PVA/Azo-OC12.

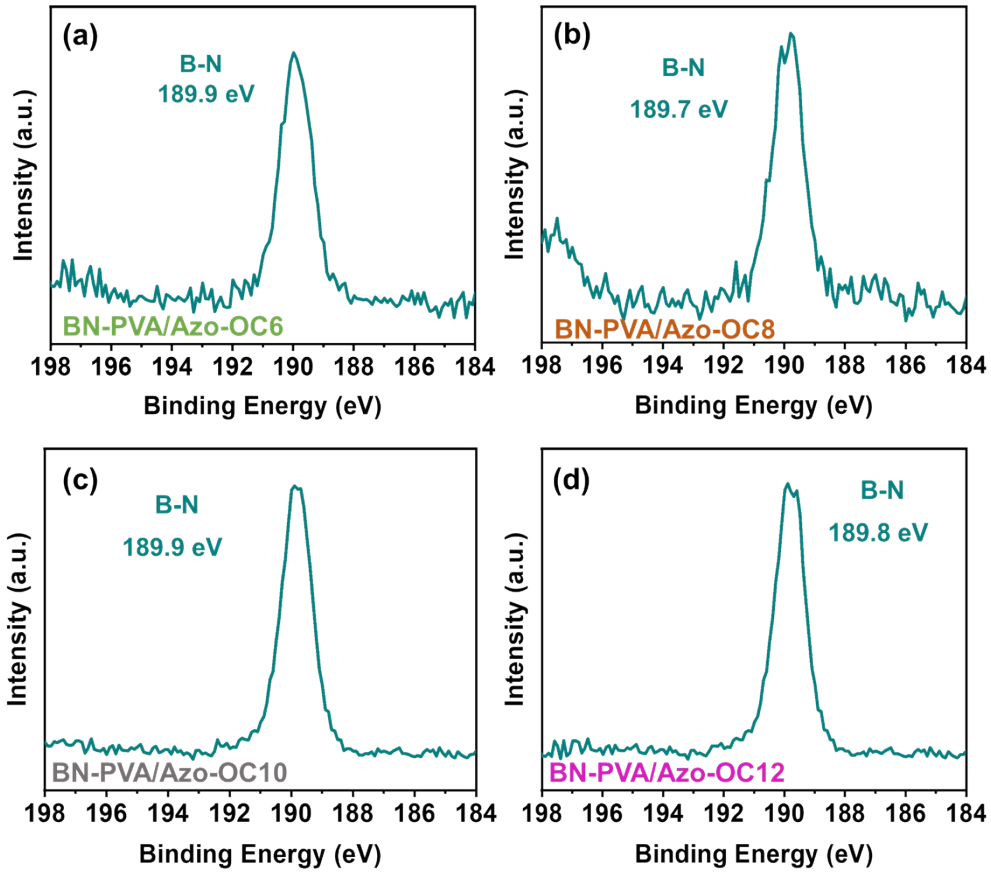

Fig. S5 B 1s XPS spectra of (a) BN-PVA/Azo-OC6, (b) BN-PVA/Azo-OC8, (c) BN-PVA/Azo-OC10, and (d) BN-PVA/Azo-OC12.

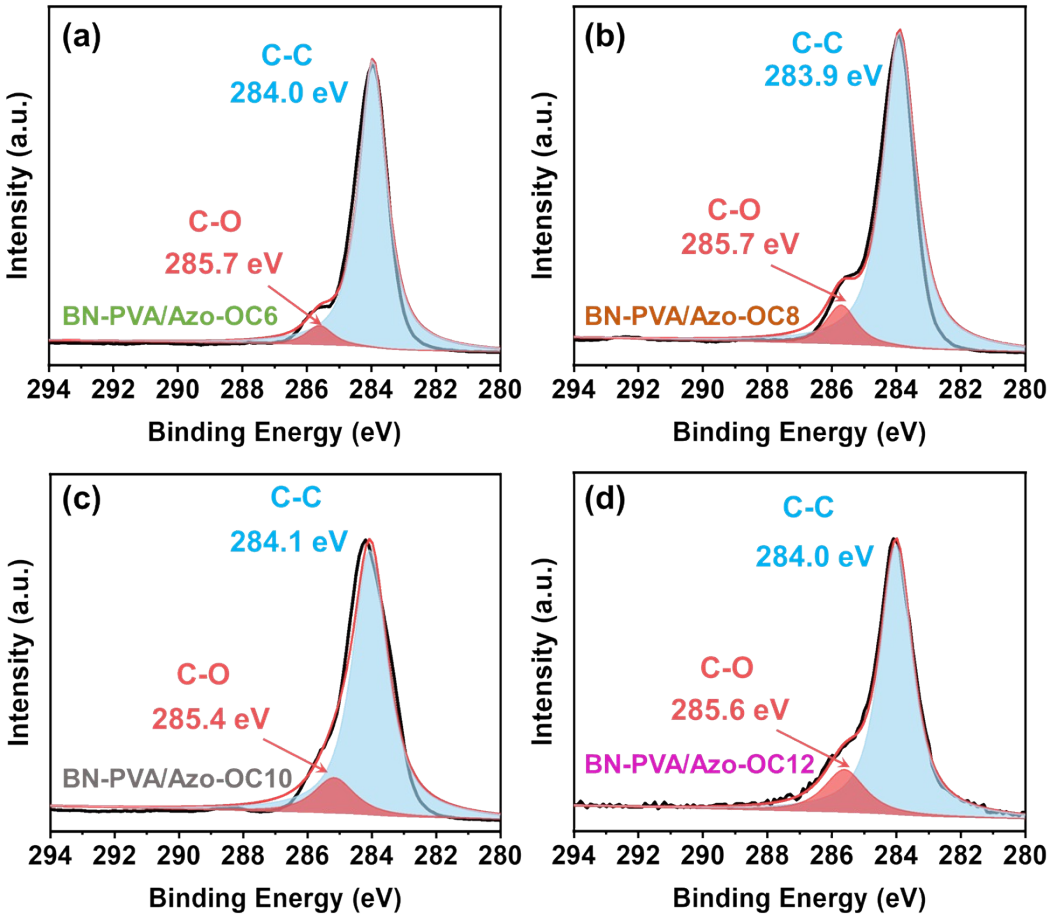

Fig. S6 C 1s XPS spectra of (a) BN-PVA/Azo-OC6, (b) BN-PVA/Azo-OC8, (c) BN-PVA/Azo-OC10, and (d) BN-PVA/Azo-OC12.

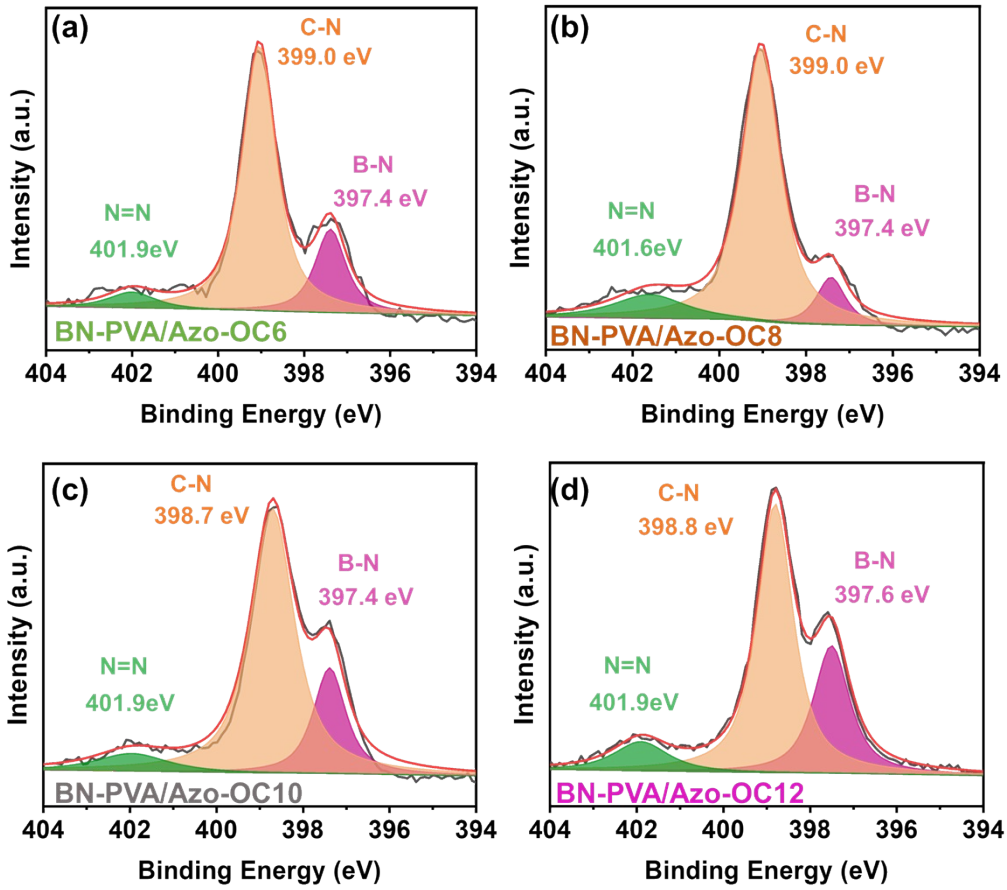

Fig. S7 N 1s XPS spectra of (a) BN-PVA/Azo-OC6, (b) BN-PVA/Azo-OC8, (c) BN-PVA/Azo-OC10, and (d) BN-PVA/Azo-OC12.

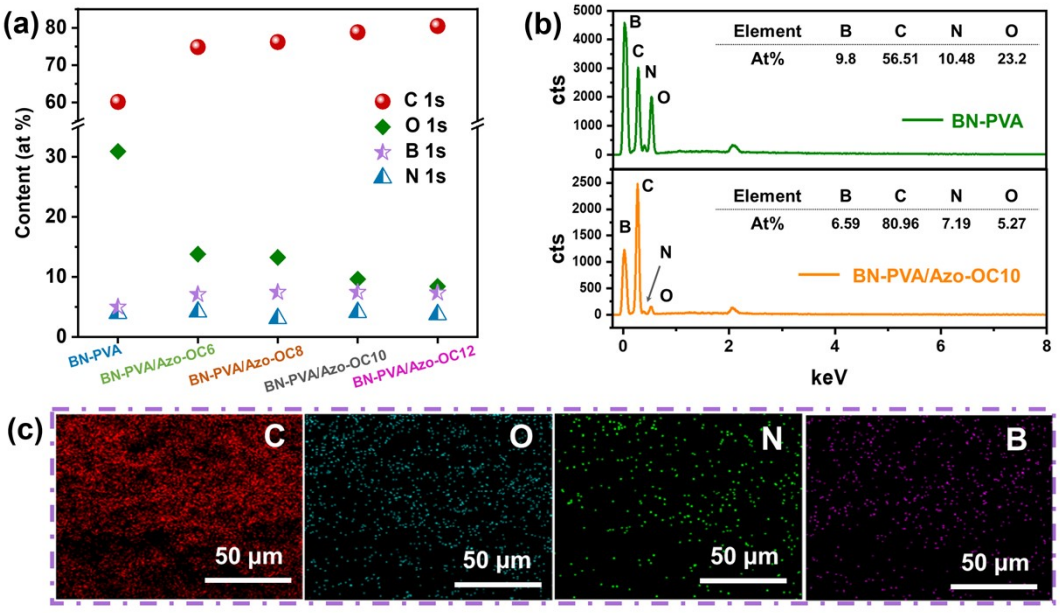

Fig. S8 (a) Composition contents of BN-PVA and BN-PVA/Azo-OC*n* (*n* = 6, 8, 10, 12)

aerogels from the XPS spectra. (b) EDS results of BN-PVA and BN-PVA/Azo-OC10. (c) The EDS mapping of the BN-PVA/Azo-OC10 composite aerogel.

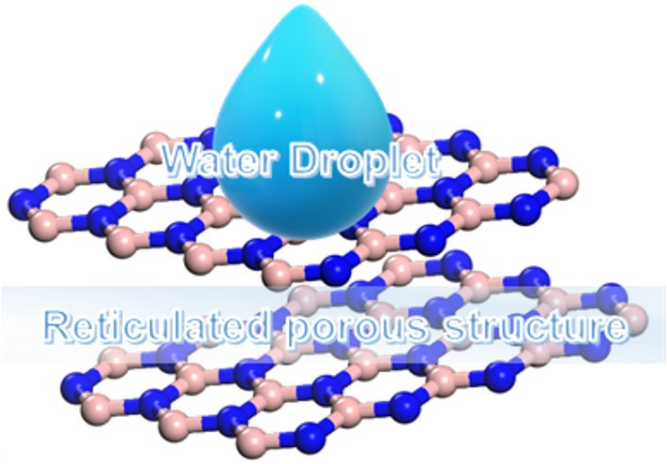

Fig. S9 Schematic illustration of the attachment state of water droplets to BN-PVA aerogel at t=0s.

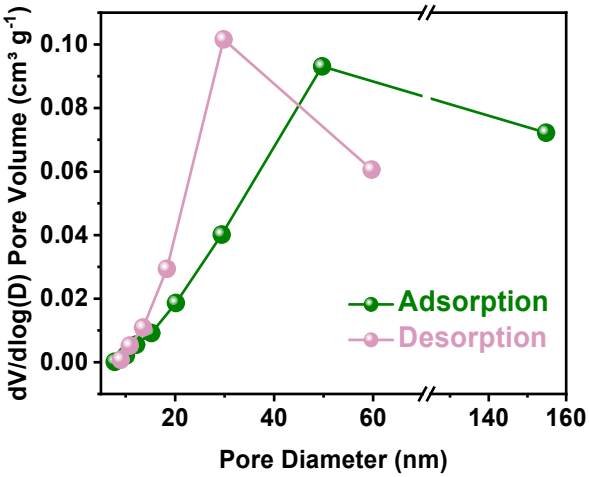

Fig. S10 The pore size distribution of BN-PVA.

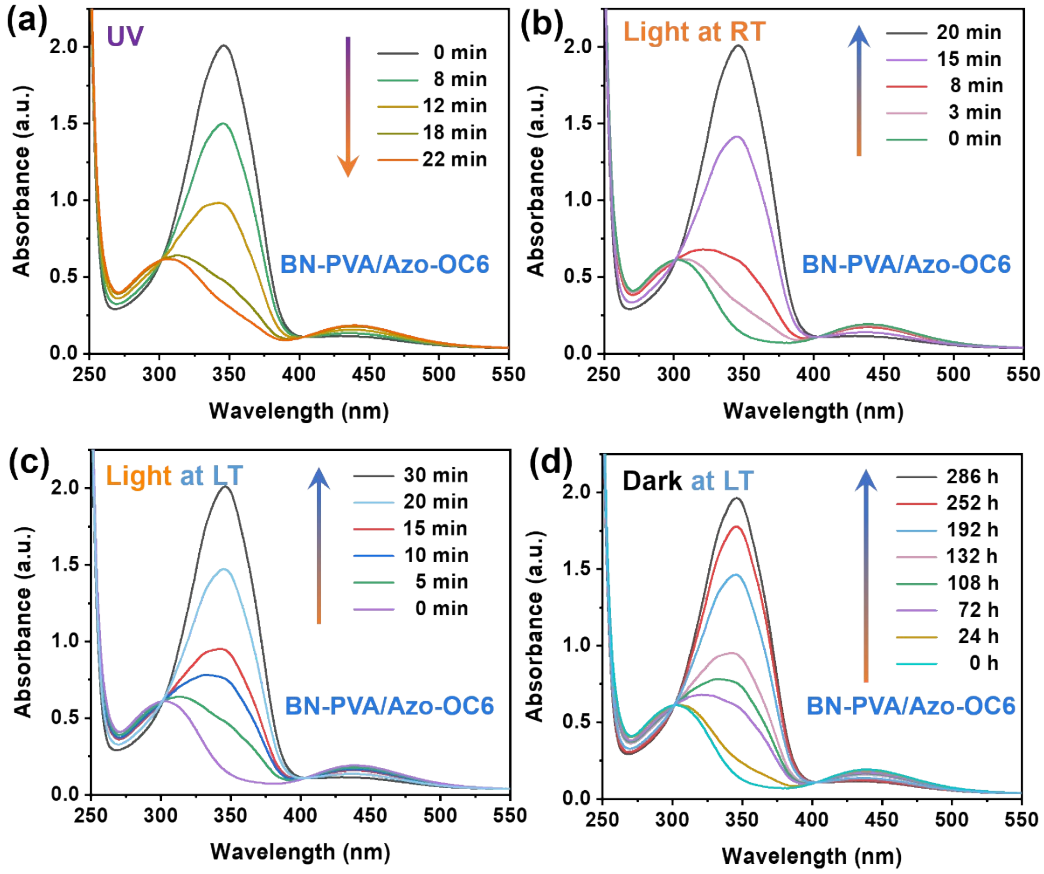

Fig. S11 Time-evolved UV-vis absorption spectra of BN-PVA/Azo-OC6 under (a) UV light irradiation, (b) light at RT (25.7 °C), (c) light at low temperature LT (-20 °C), and (d) dark environment at LT (-20 °C).

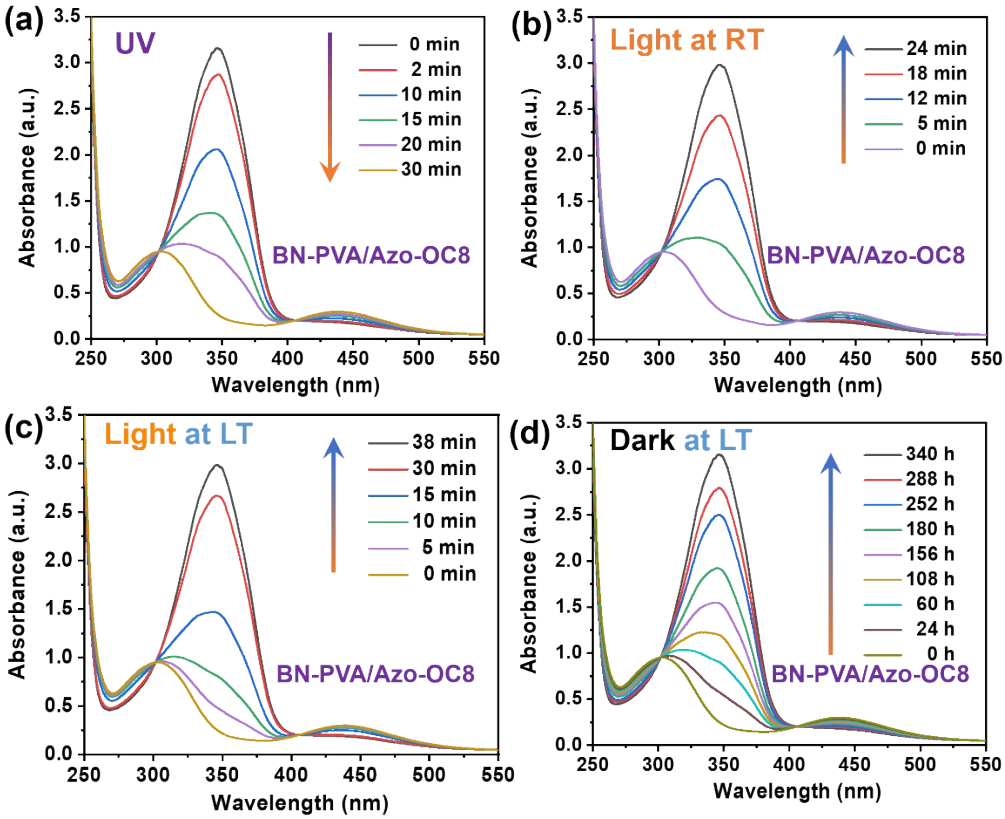

Fig. S12 Time-evolved UV-vis absorption spectra of BN-PVA/Azo-OC8 under (a) UV light irradiation, (b) light at RT (25.7 °C), (c) light at low temperature LT (-20 °C), and (d) dark environment at LT (-20 °C).

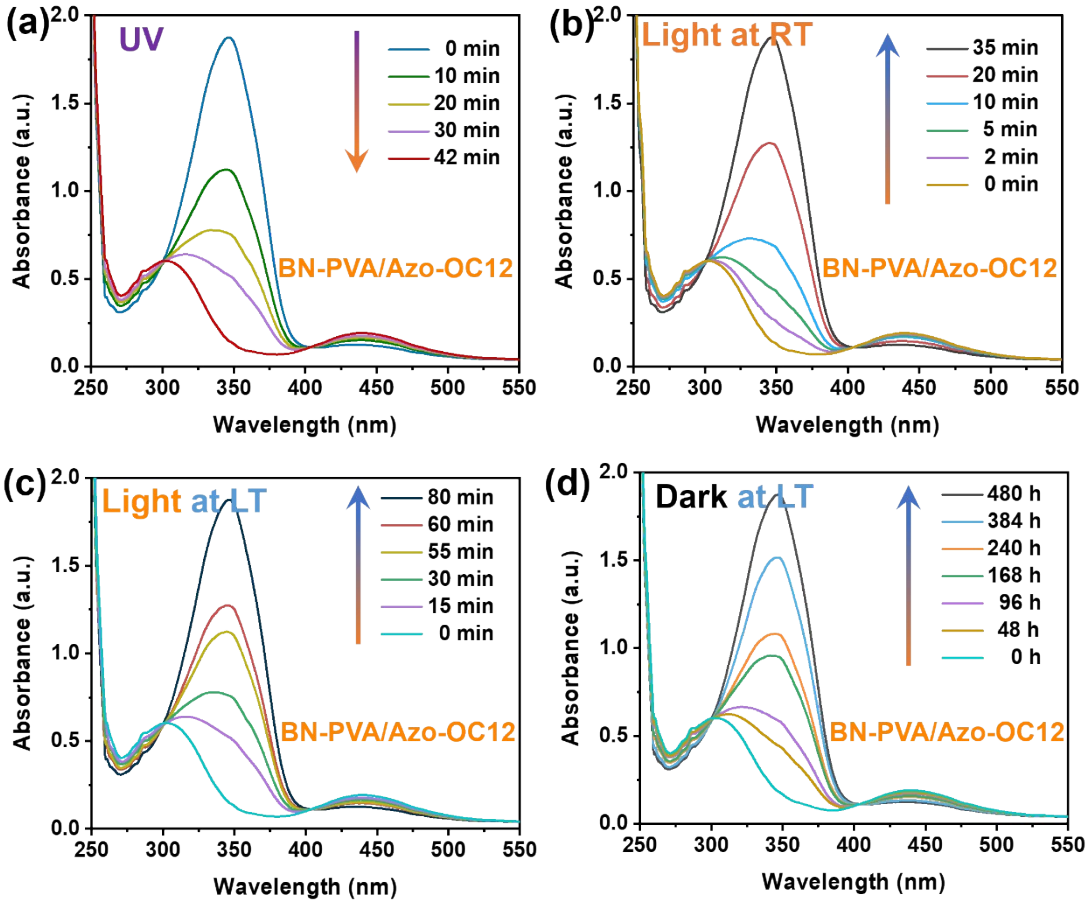

Fig. S13 Time-evolved UV-vis absorption spectra of BN-PVA/Azo-OC12 under (a) UV light irradiation, (b) light at RT (25.7 °C), (c) light at low temperature LT (-20 °C), and (d) dark environment at LT (-20 °C).

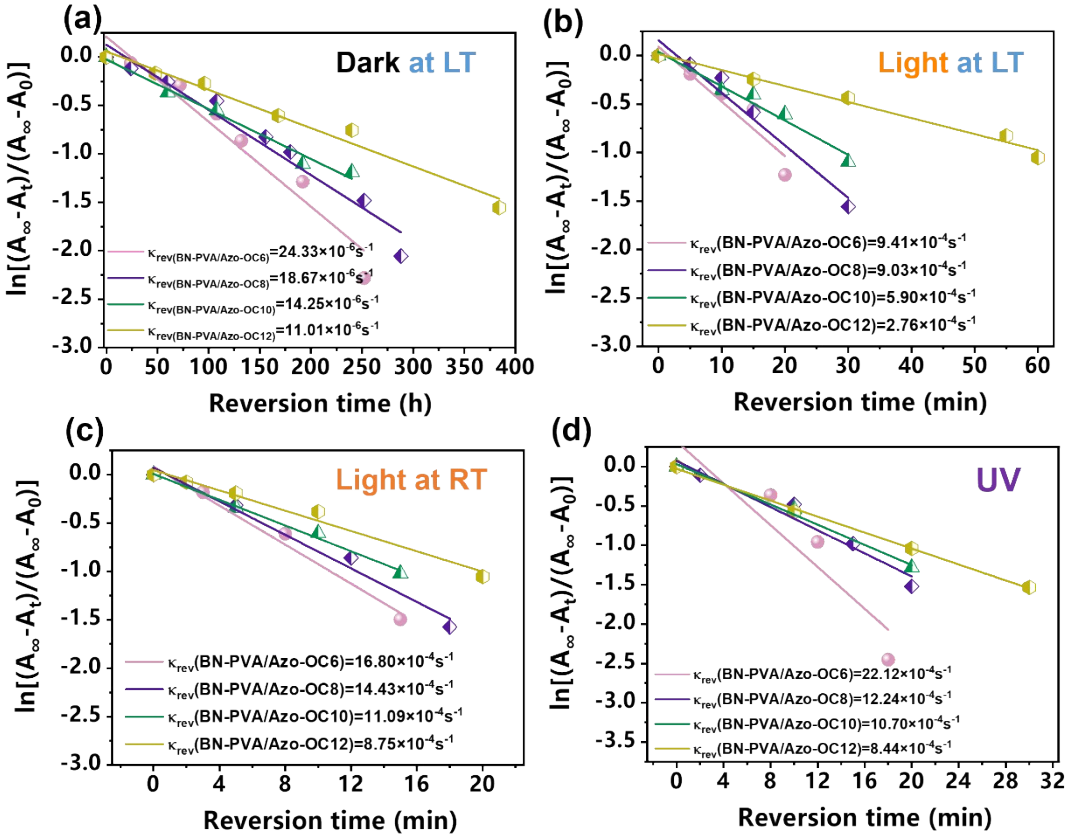

Fig. S14 (a)-(c) The *Z*-to-*E* isomerization rate constants (κ_{rev}) of BN-PVA/Azo-OC*n* (*n*=6, 8, 10, 12) under dark at LT, light at LT, and light at RT conditions, respectively. (d) The *E*-to-*Z* isomerization rate constants (κ_{rev}) of BN-PVA/Azo-OC*n* (*n*=6, 8, 10, 12) under UV light conditions.

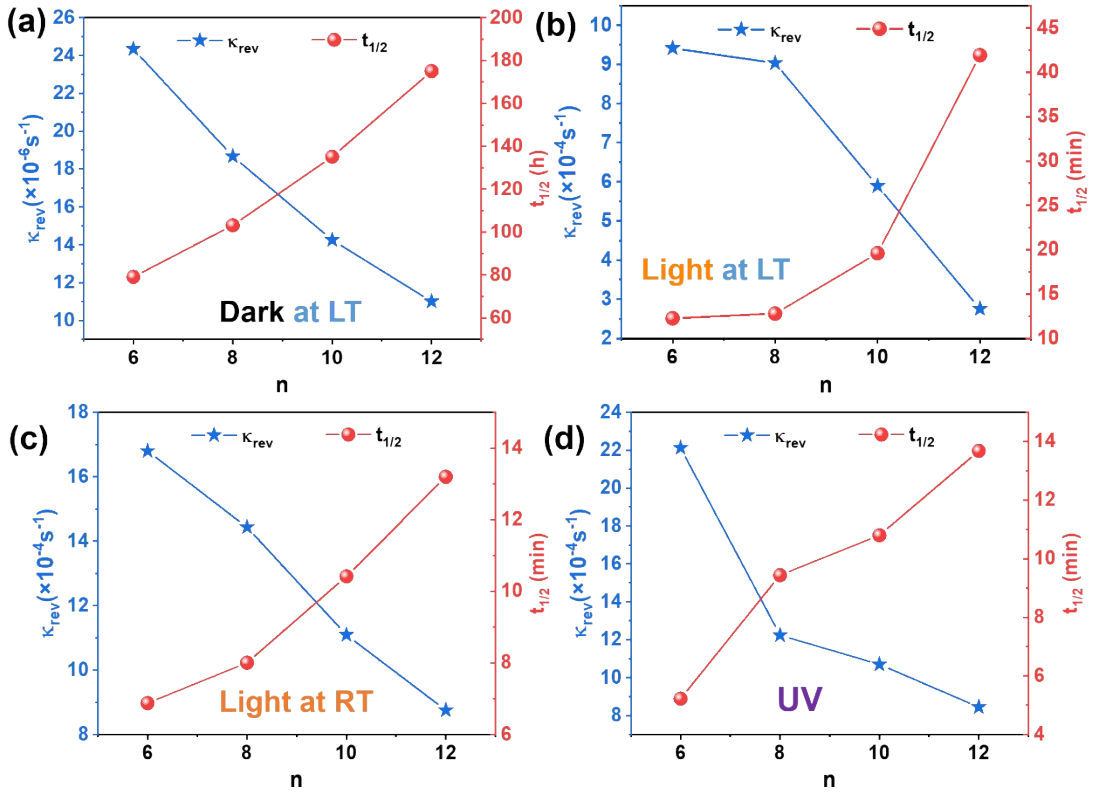

Fig. S15 (a)-(c) Relationship between the *Z*-to-*E* isomerization rate constants (κ_{rev}), half-lives ($t_{1/2}$), and different Alkoxy chain length (*n*, *n*=6, 8, 10, 12) under dark at LT, light at LT, and light at RT conditions, respectively. (d) The *E*-to-*Z* isomerization under UV light conditions.

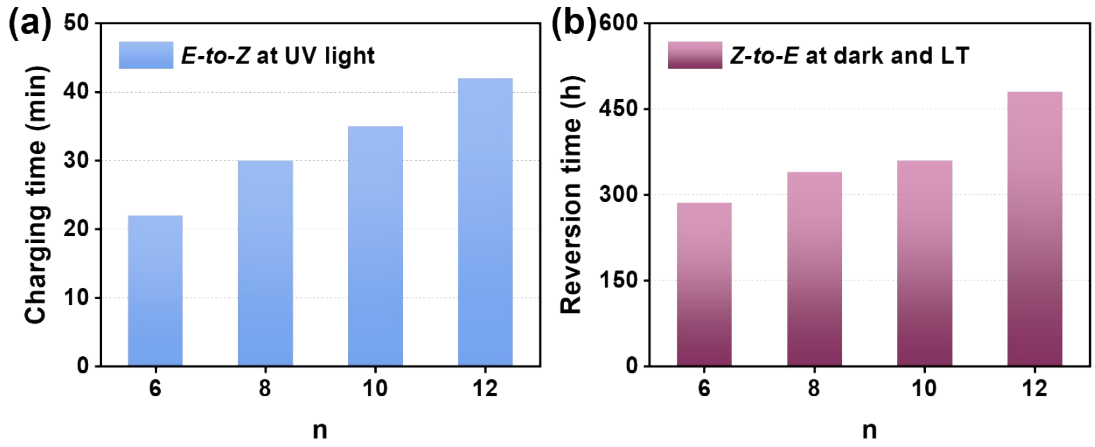

Fig. S16 (a) The bar chart of charging time of BN-PVA/Azo-OC*n* (*n*=6, 8, 10, 12) under UV light (365 nm). (b) The bar chart of reversion time of BN-PVA/Azo-OC*n* (*n*=6, 8, 10, 12) under dark and LT (-20 °C) conditions.

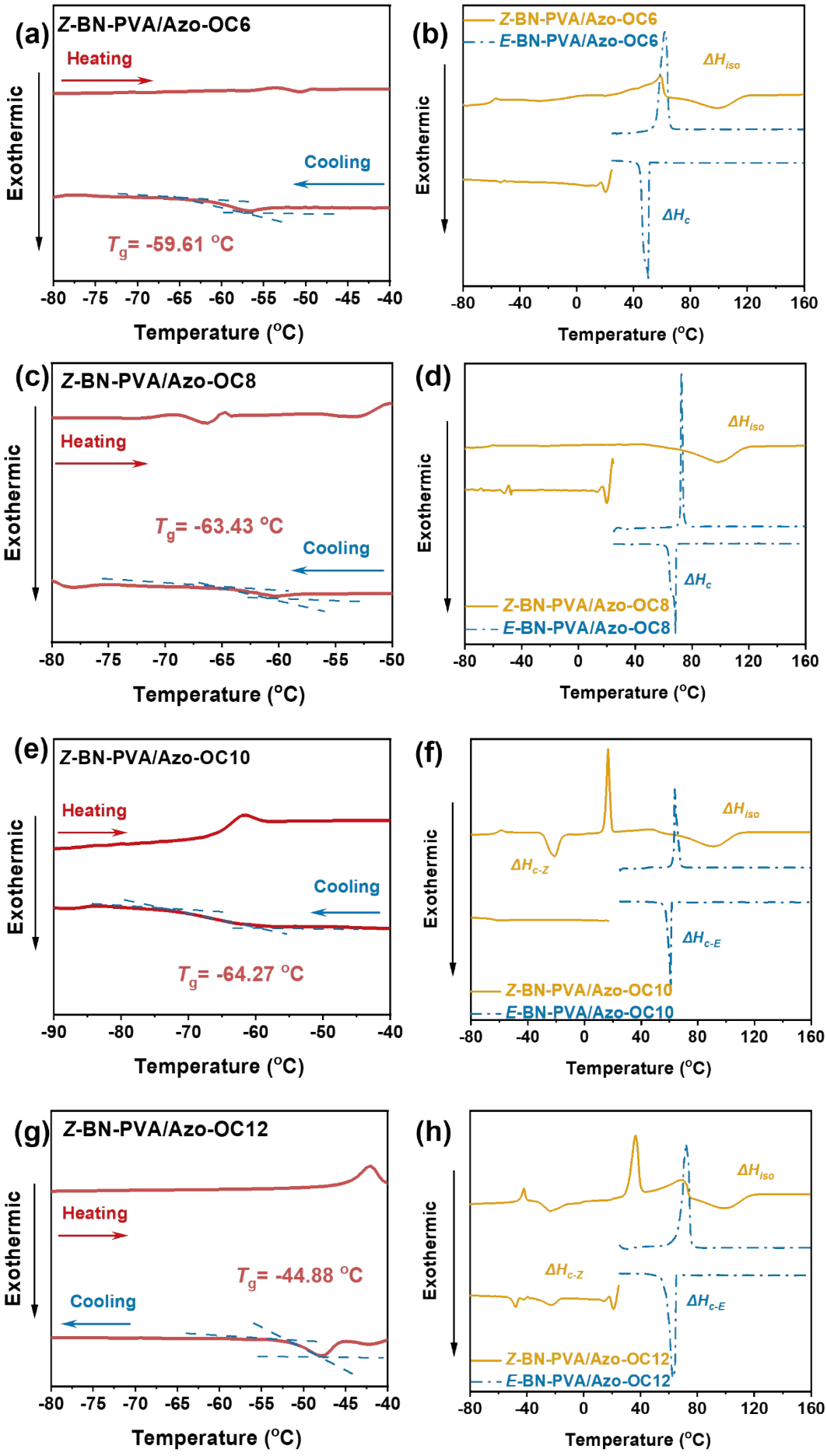
(a)
Z-BN-PVA/Azo-OC6
Heating
Cooling
T_g= -59.61 °C
Exothermic
Temperature (°C)
(b)
Z-BN-PVA/Azo-OC6
E-BN-PVA/Azo-OC6
ΔH_{iso}
ΔH_c
Exothermic
Temperature (°C)
(c)
Z-BN-PVA/Azo-OC8
Heating
T_g= -63.43 °C
Cooling
Exothermic
Temperature (°C)
(d)
ΔH_{iso}
ΔH_c
Z-BN-PVA/Azo-OC8
E-BN-PVA/Azo-OC8
Exothermic
Temperature (°C)
(e)
Z-BN-PVA/Azo-OC10
Heating
Cooling
T_g= -64.27 °C
Exothermic
Temperature (°C)
(f)
ΔH_{iso}
ΔH_{c-Z}
ΔH_{c-E}
Z-BN-PVA/Azo-OC10
E-BN-PVA/Azo-OC10
Exothermic
Temperature (°C)
(g)
Z-BN-PVA/Azo-OC12
Heating
T_g= -44.88 °C
Cooling
Exothermic
Temperature (°C)
(h)
ΔH_{iso}
ΔH_{c-Z}
ΔH_{c-E}
Z-BN-PVA/Azo-OC12
E-BN-PVA/Azo-OC12
Exothermic
Temperature (°C)

Fig. S17 DSC curves on T_g of (a) *Z*-BN-PVA/Azo-OC6, (c) *Z*-BN-PVA/Azo-OC8, (e) *Z*-BN-PVA/Azo-OC10, and (g) *Z*-BN-PVA/Azo-OC12 from -80 to -40 °C at a heating and cooling rate of 10 °C min^{-1}. DSC curves of (b) *E*-BN-PVA/Azo-OC6 (dotted blue line) and *Z*-BN-PVA/Azo-OC6 (straight yellow line), (d) *E*-BN-PVA/Azo-OC8 and *Z*-BN-PVA/Azo-OC8, (f) *E*-BN-PVA/Azo-OC10 and *Z*-BN-PVA/Azo-OC10 and (h) *E*-BN-PVA/Azo-OC12 and *Z*-BN-PVA/Azo-OC12 with the cooling and heating rate of 10 °C min^{-1}.

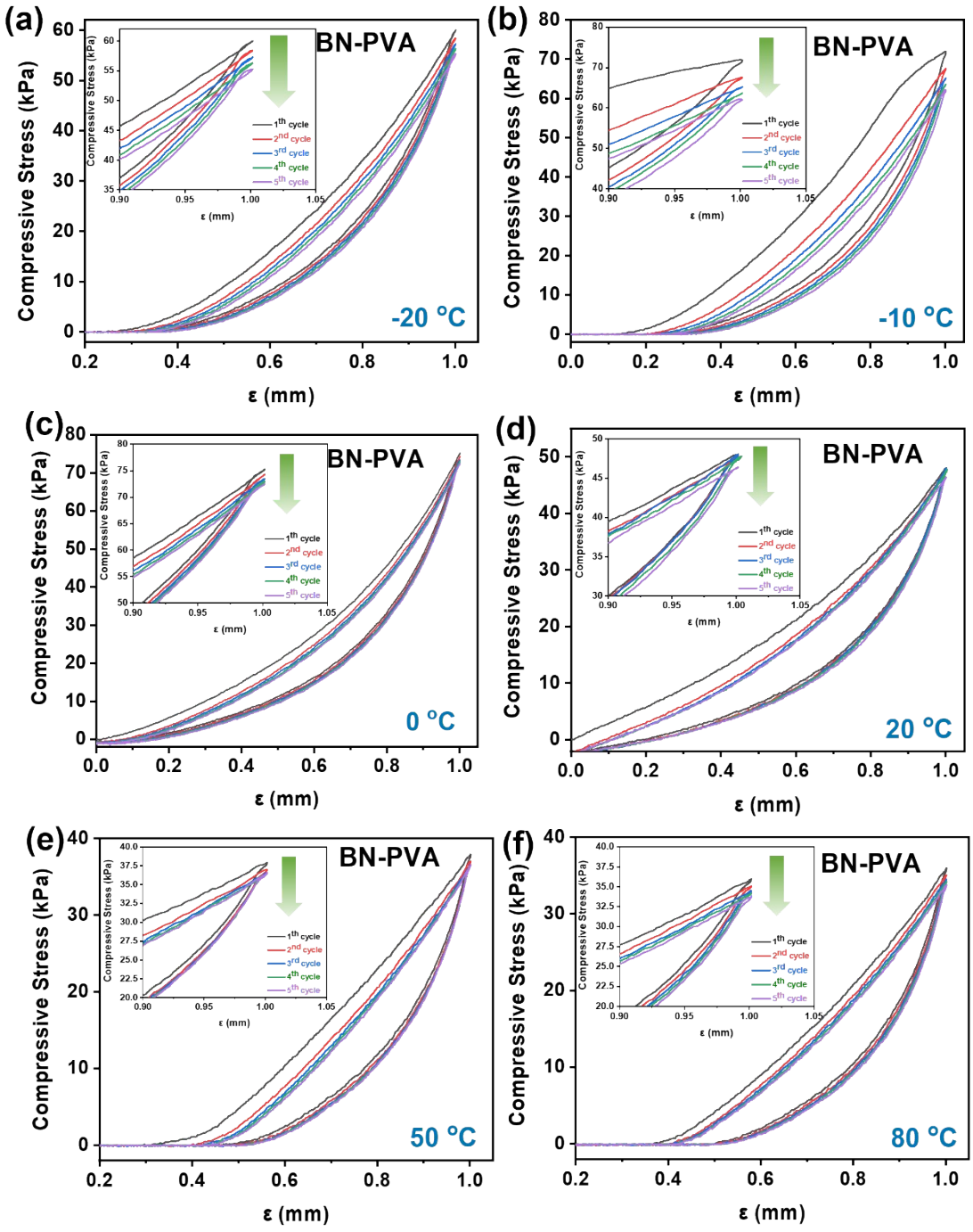

Fig. S18 Comparative compression curves of BN-PVA aerogels at different

temperatures (-20°C to 80°C). (a) -20 °C, and insert graph is the magnified view of deformation (ε) between 0.9-1.05 mm, (b) -10 °C, and insert graph is the magnified view of deformation (ε) between 0.9-1.05 mm, (c) 0 °C, and insert graph is the magnified view of deformation (ε) between 0.9-1.05 mm, (d) 20°C, and insert graph is the magnified view of deformation (ε) between 0.9-1.05 mm, (e) 50 °C, and insert graph is the magnified view of deformation (ε) between 0.9-1.05 mm, (f) 80 °C, and insert graph is the magnified view of deformation (ε) between 0.9-1.05 mm.

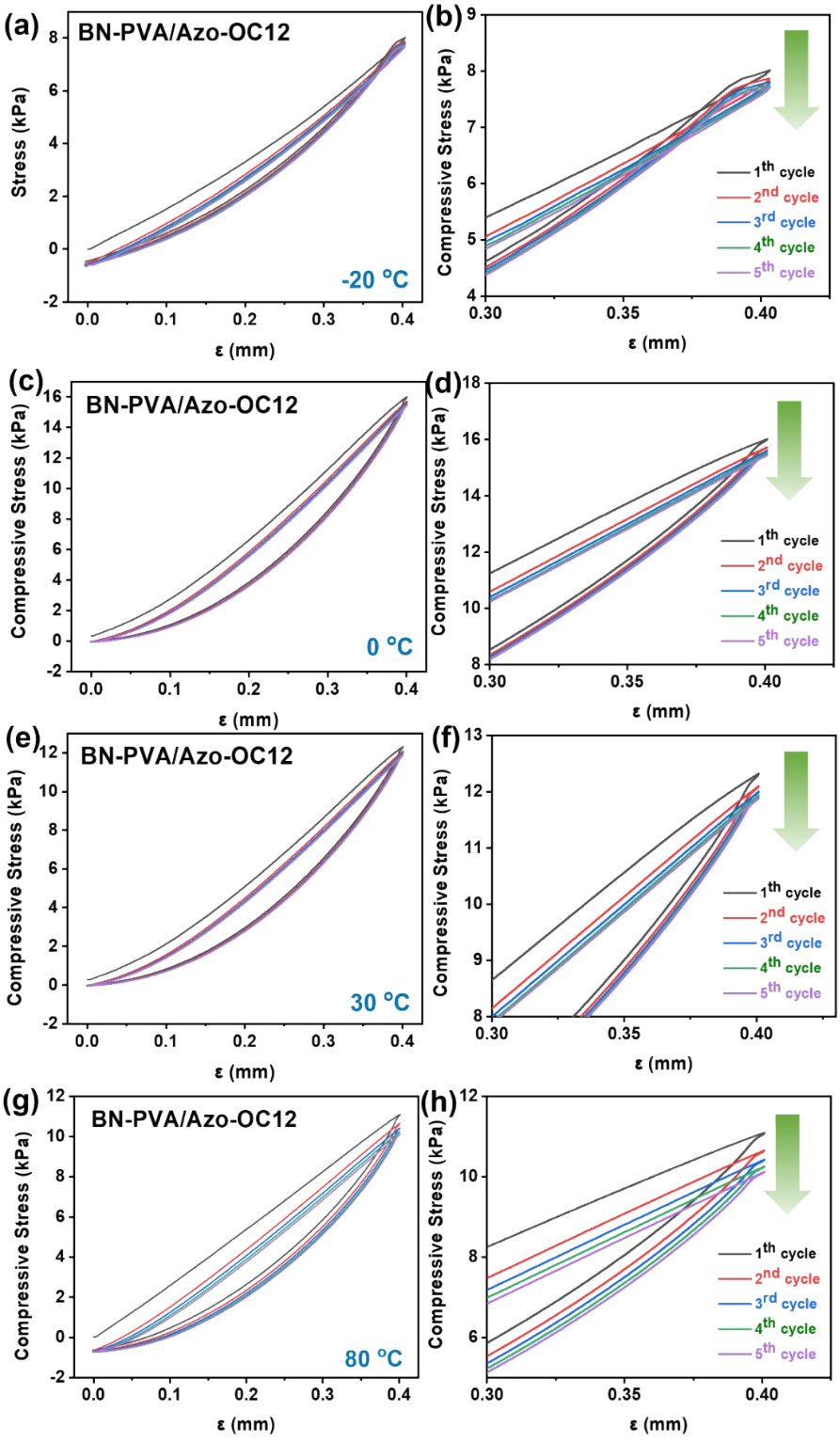

Fig. S19 Comparative compression curves of BN-PVA/Azo-OC12 composite aerogel at different temperatures. (a) -20 °C, (b) the magnified view at -20°C, (c) 0 °C, (d) the magnified view at 0°C, (e) 30 °C, (f) the magnified view at 30°C, (g) 80 °C, (h) the magnified view at 80°C.

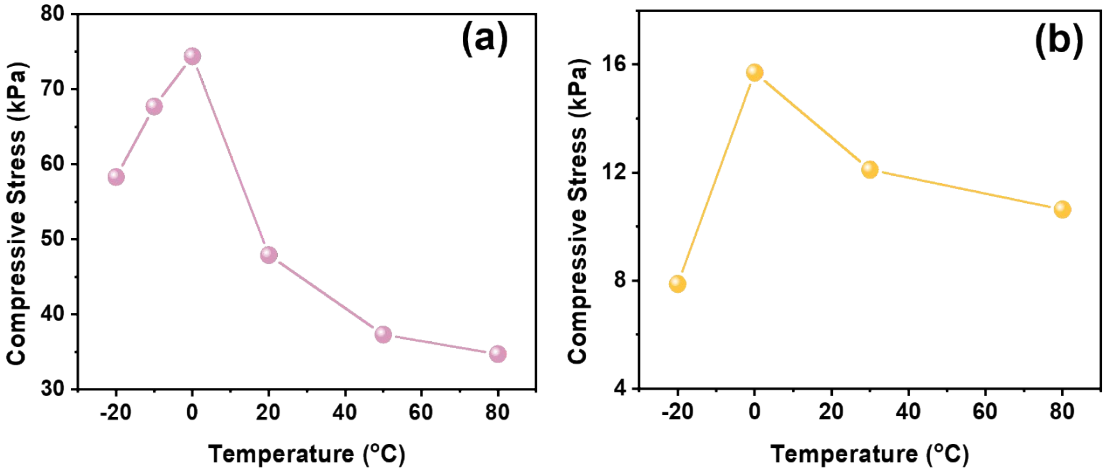

Fig. S20 Comparative curves of compressive stress and deformation (ε) of BN-PVA aerogel (a) and BN-PVA/Azo-OC12 composite aerogel (b) at different temperatures.

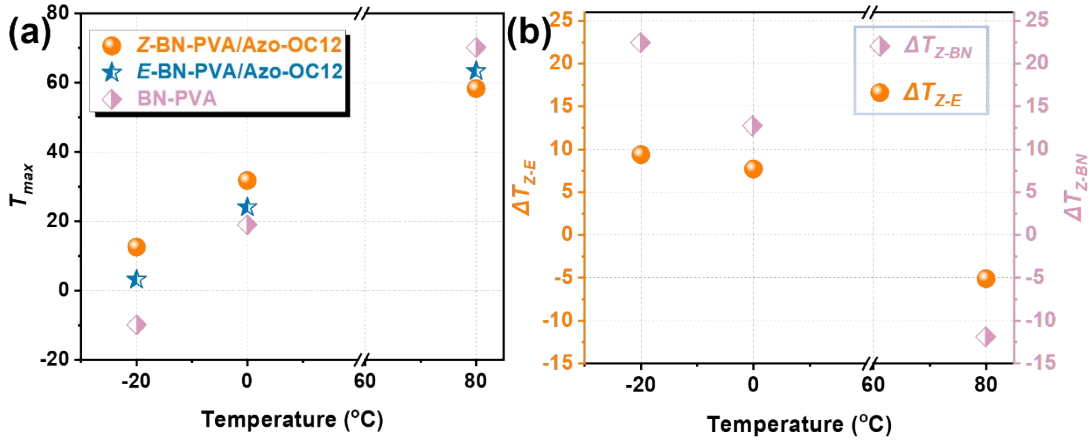

Fig. S21 (a) Statistical comparison plots of the maximum values of exothermic temperatures (T_{max}) of BN-PVA, *E*-BN-PVA/Azo-OC12, and *Z*-BN-PVA/Azo-OC12 at -20°C, 0°C, and 80°C. (b) Statistical plots of the exothermic temperature difference between *E*-BN-PVA/Azo-OC12 and *Z*-BN-PVA/Azo-OC12 ($\Delta T_{Z\text{-}E}$), BN-PVAand *Z*-BN-PVA/Azo-OC12 ($\Delta T_{Z\text{-}BN}$) at the same temperature.

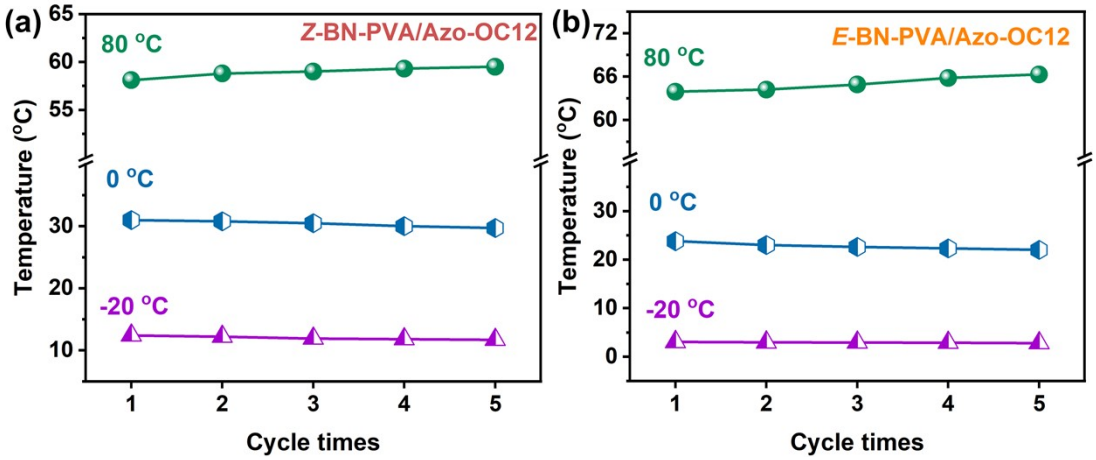

Fig. S22. The maximum exothermic temperature statistics graph of heat release after each cycle in 5 charge-discharge cycles. (a) *Z*-BN-PVA/Azo-OC12; (b) *E*-BN-PVA/Azo-OC12.

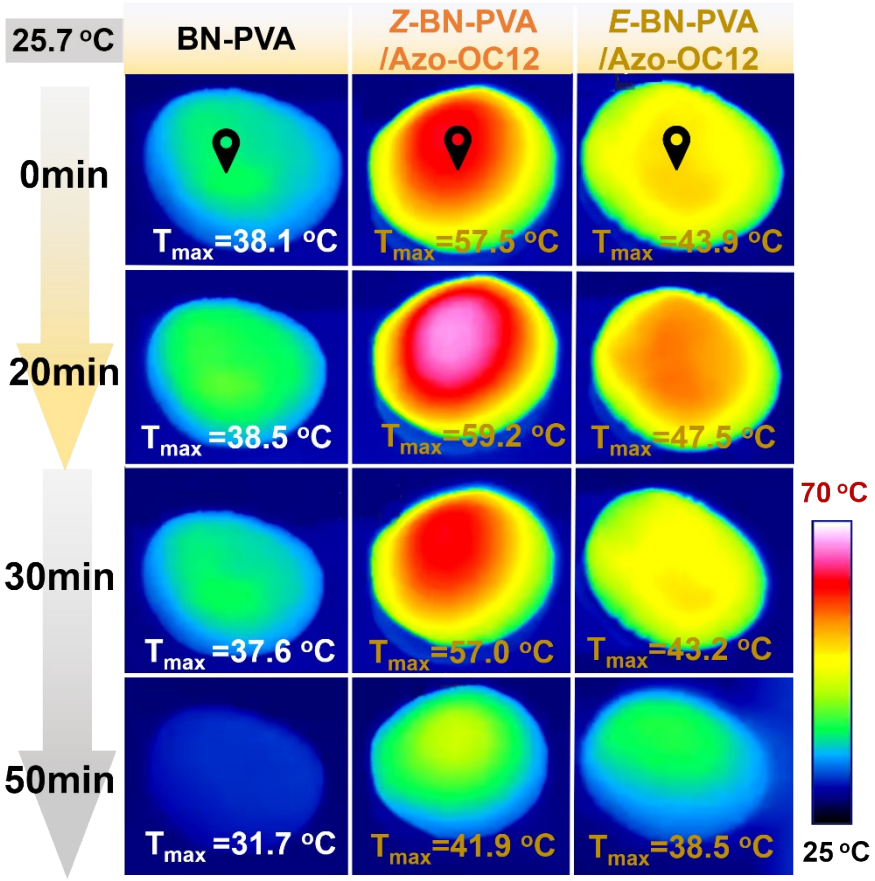

Fig. S23 Heat release at room temperature (25.7 °C). Time-evolved IR thermal imaging with BN-PVA, *Z*-BN-PVA/Azo-OC12 and *E*-BN-PVA/Azo-OC12 for one cycle, including Sunlight irradiation (yellow arrow) for 20 min and natural exotherm (gray arrow) for the succeeding 18 min. T_{max} is the maximum temperature displayed in the infrared thermal imager.

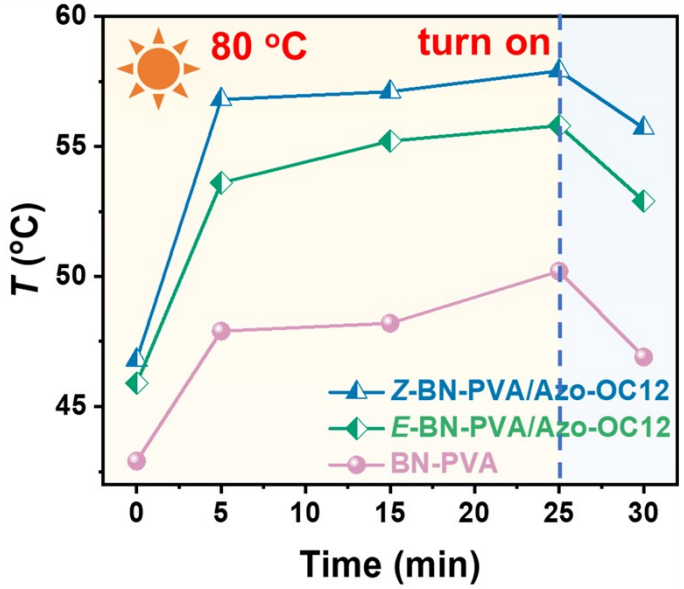

Fig. S24 Plot of exothermic temperature (*T*) versus time at high temperature (80 °C) for BN-PVA, *Z*-BN-PVA/Azo-OC12 and *E*-BN- PVA/Azo-OC12.

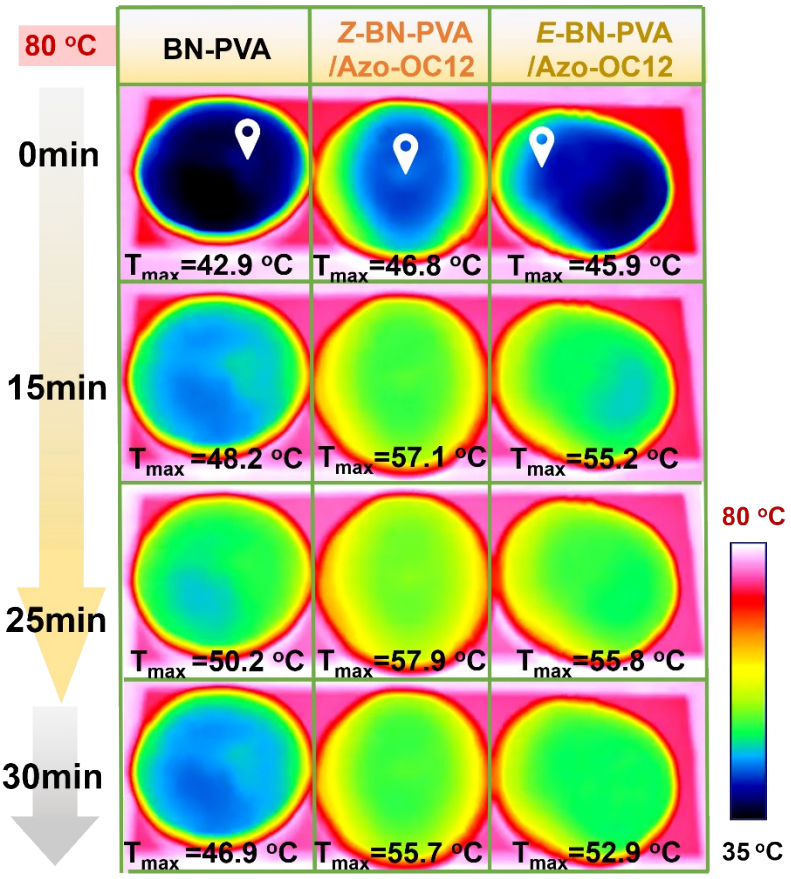

Fig. S25 Heat release at high temperature (80 °C). Time-evolved IR thermal imaging with BN-PVA, *Z*-BN-PVA/Azo-OC12 and *E*-BN-PVA/Azo-OC12 for one cycle, including Sunlight irradiation (yellow arrow) for 25 min and natural exotherm (gray arrow) for the succeeding 5 min. T_{max} is the maximum temperature displayed in the infrared thermal imager.

Supplementary Tables

Table S1 The porosity (*P*) and the filling ratio (*P*) of BN-PVA/Azo-OC*n* (*n* = 6, 8, 10, 12) aerogels.

Samples	*P* (%)	*F* (%)
BN-PVA/Azo-OC6	90.14	80.02
BN-PVA/Azo-OC8	91.24	81.21
BN-PVA/Azo-OC10	93.89	83.75
BN-PVA/Azo-OC12	91.10	81.77

Table S2 Element content of BN-PVA and BN-PVA/Azo-OC*n* (*n* = 6, 8, 10, 12) aerogels.

Sample	Element content (%)			
	C	N	O	B
BN-PVA	60.11	5.02	30.9	3.95
BN-PVA/Azo-OC6	74.82	7.11	13.79	4.18
BN-PVA/Azo-OC8	76.18	7.46	13.26	3.09
BN-PVA/Azo-OC10	78.79	7.45	9.64	4.11
BN-PVA/Azo-OC12	80.46	7.37	8.43	3.74

Table S3 Total specific surface area, micropore specific surface area, pore volume, micropore volume percentage, and average pore diameter of BN-PVA aerogel.

Sample	Surface Area ($m^2 g^{-1}$)	Micropore Area ($m^2 g^{-1}$)	Micropore volume ($cm^3 g^{-1}$)	Microporous volume percentage ($cm^3 g^{-1}$)	Average pore diameter (nm)
BN-PVA	70.61	9.89	0.094	15.96%	52.86

Table S4 The *Z*-to-*E* and *E*-to-*Z* isomerization rate constants (κ_{rev}) and half-lives ($t_{1/2}$) of BN-PVA/Azo-OC*n* (*n* = 6, 8, 10, 12) under dark at LT, light at LT, light at RT, and UV light conditions.

Samples	Dark at LT		Light at LT		Light at RT		UV	
	κ_{rev}(×10^{-6}s^{-1})	$t_{1/2}$(h)	κ_{rev}(×10^{-4}s^{-1})	$t_{1/2}$(min)	κ_{rev}(×10^{-4}s^{-1})	$t_{1/2}$(min)	κ_{rev}(×10^{-4}s^{-1})	$t_{1/2}$(min)
BN-PVA/Azo-OC6	24.33	79.17	9.41	12.27	16.80	6.88	22.12	5.22
BN-PVA/Azo-OC8	18.67	103.15	9.03	12.78	14.43	8.00	12.24	9.44
BN-PVA/Azo-OC10	14.25	135.12	5.90	19.60	11.09	10.42	10.70	10.80
BN-PVA/Azo-OC12	11.01	175.04	2.76	41.93	8.75	13.20	8.44	13.68

Table S5 The T_c ($T_{c\text{-}E}$ and $T_{c\text{-}Z}$), ΔH_c ($\Delta H_{c\text{-}E}$ and $\Delta H_{c\text{-}Z}$), T_{iso}, ΔH_{iso}, T_g, and ΔH_{total} of BN-PVA/Azo-OC*n* (*n* = 6, 8, 10, 12, respectively).

Samples		T_c (°C)	ΔH_c (J g^{-1})	T_{iso} (°C)	ΔH_{iso} (J g^{-1})	T_g (°C)	ΔH_{total} (J g^{-1})
BN-PVA/Azo-OC6	*Z*-Azo-OC6	-	-	95.16	144.5	-59.61	239.1
	E-Azo-OC6	50.86	94.6	-	-	-	
BN-PVA/Azo-OC8	*Z*-Azo-OC8	-	-	95.42	138.8	-63.43	240.3
	E-Azo-OC8	58.54	101.5	-	-	-	
BN-PVA/Azo-OC10	*Z*-Azo-OC10	-21.28	33.67	98.04	129.0	-64.27	282.5
	E-Azo-OC10	60.73	119.8	-	-	-	
BN-PVA/Azo-OC12	*Z*-Azo-OC12	-13.35	42.88	99.42	112.7	-44.88	284.7
	E-Azo-OC12	62.85	129.1	-	-	-	

Table S6 The $T_{Z\text{-}max}$, $T_{E\text{-}max}$, $T_{BN\text{-}max}$, $\Delta T_{Z\text{-}E}$, and $\Delta T_{Z\text{-}BN}$ at -20 °C, 0 °C, and 80 °C measured by thermocouples for BN-PVA aerogel and BN-PVA/Azo-OC12 composite aerogel.

Temperature (°C)	$T_{Z\text{-}max}$ (°C)	$T_{E\text{-}max}$ (°C)	$T_{BN\text{-}max}$ (°C)	$\Delta T_{Z\text{-}E}$ (°C)	$\Delta T_{Z\text{-}BN}$ (°C)
-20	12.55	3.16	-9.9	9.39	22.45
0	31.75	24.05	19	7.7	12.75
80	58.3	63.4	70.18	-5.1	-11.88

Table S7 The T_{max}, T_{min}, and ΔT_{total} of BN-PVA, *E*-BN-PVA/Azo-OC12, and *Z*-BN-PVA/Azo-OC12 measured by thermocouples during the warming process from -20 °C to 80 °C.

	T_{max} (°C)	T_{min} (°C)	ΔT_{total} (°C)
BN-PVA	70.4	-8.7	79.1
***E*-BN-PVA/Azo-OC12**	63.84	4.43	68.27
***Z*-BN-PVA/Azo-OC12**	58.4	7.1	65.5

Table S8 The surface temperatures of BN-PVA, E-BN-PVA/Azo-OC12, and Z-BN-PVA/Azo-OC12 at -20 °C as a function of time.

Time (min)	$T_{BN\text{-}PVA}$(°C)	$T_{E\text{-}BN\text{-}PVA/Azo\text{-}OC12}$(°C)	$T_{Z\text{-}BN\text{-}PVA/Azo\text{-}OC12}$(°C)
0 min	-5	-5	-5.1
10 min	-4.8	10.4	13.7
35 min	7.3	21.3	29.2
60 min	5.8	15.1	18.8
80 min	3.6	4.3	4.6

Table S9 The surface temperatures of BN-PVA, E-BN-PVA/Azo-OC12, and Z-BN-PVA/Azo-OC12 at -25.7 °C as a function of time.

Time (min)	BN/PVA	*E*-BN-PVA/Azo-OC12	*Z*-BN-PVA/Azo-OC12
0min	38.1	43.9	57.5
5 min	39.9	50.5	60.1
20 min	38.5	47.5	59.2
30 min	37.6	43.2	57
50 min	31.7	38.5	41.9

Table S10 The surface temperatures of BN-PVA, E-BN-PVA/Azo-OC12, and Z-BN-PVA/Azo-OC12 at 80 °C as a function of time.

Time (min)	BN/PVA	*E*-BN-PVA/Azo-OC12	*Z*-BN-PVA/Azo-OC12
0min	42.9	45.9	46.8
5 min	47.9	53.6	56.8
15 min	48.2	55.2	57.1
25 min	50.2	55.8	57.9
30 min	46.9	52.9	55.7

Supplementary Equations

Equation S1

$$V_1 = r^2 \times h$$

$$V_2 = \frac{m}{\rho}$$

$$P = \frac{V_1 - V_2}{V_1}$$

where *P* is the porosity, V_1 is the total volume of the BN-PVA aerogel, *r* is the diameter of the aerogel, and *h* is the thickness of the aerogel; V_2 is the volume of BN-PVA, *m* is the mass of the aerogel, and ρ is the density of BN-PVA.

Equation S2

$$V_3 = \frac{m_{total}}{\rho_1}$$

$$F = \frac{V_3}{V_1 - V_2}$$

where *F* represents the filling ratio, V_3 is the volume of filled BN-PVA composite aerogel, *m* is the mass of the filled composite aerogel, and ρ is the density of the filled photo-controlled PCMs.

Equation S3 [1]

$$\ln\left(\frac{A_\infty - A_t}{A_\infty - A_0}\right) = -\kappa_{rev} t$$

Where A_0 is the absorption intensity of π-π* transition peak in the *Z*-Azo-OCn irradiated by UV light, A_t is the absorption intensity of π-π* transition peak reversing for "*t*" time, A_∞ is the absorption intensity of π-π* transition peak after complete Z-reversion and κ_{rev} is *Z*-to-*E* isomerization rate constants under blue light or in darkness.

Equation S4 [2]

$$t_{1/2} = \frac{\ln 2}{\kappa_{rev}}$$

Where $t_{1/2}$ is the dark half-lives and κ_{rev} is *Z*-to-*E* isomerization rate constants under blue light or in darkness.

Equation S5 [3]

$$\Delta H_{total-1} = \Delta H_{iso} + \Delta H_{c-E}$$

Where $\Delta H_{total-1}$ is the total energy density, ΔH_{c-E} is the crystallization enthalpies of the *E*-isomer, and the ΔH_{iso} is the isomerization enthalpies. This formula is applied to two heat release processes of BN-PVA/Azo-OC6 and BN-PVA/Azo-OC8.

Equation S6 [3]

$$\Delta H_{total-2} = \Delta H_{c-E} + \Delta H_{c-Z} + \Delta H_{iso}$$

Where $\Delta H_{total-2}$ is the total energy density, ΔH_{c-E} is the crystallization enthalpies of the *E*-isomer, ΔH_{c-Z} is the crystallization enthalpies of the *Z*-isomer, and the ΔH_{iso} is the isomerization enthalpies. This formula is applied to three heat release processes of BN-PVA/Azo-OC10 and BN-PVA/Azo-OC12.

Notes and references

[1] Q. Yan, Y. Zhang, Y. Dang, Y. Feng, W. Feng. Solid-state high-power photo heat output of 4-((3,5-dimethoxyaniline)-diazenyl)-2-imidazole/graphene film for thermally controllable dual data encoding/reading. *Energy Stor. Mater.* 2020; 24: 662-669.

[2] H. Wang, Y. Feng, J. Gao, W. Fang, J. Ge, X. Yang, F. Zhai, Y. Yu, W. Feng. Metallic-ion controlled dynamic bonds to co-harvest isomerization energy and bond enthalpy for high-energy output of flexible self-heated textile. *Adv. Sci*. 2022; 9: 2201657.

[3] H. Liu, J. Tang, L. Dong, H. Wang, T. Xu, W. Gao, F. Zhai, Y. Feng, W. Feng. Optically triggered synchronous heat release of phase-change enthalpy and photo-thermal energy in phase-change materials at low temperatures. *Adv. Funct. Mater.* 2020; 31: 2008496.